Predicting the amount of carbon in carbon nanotubes grown by CH_4 rf plasmas

Atsushi Okita, Yoshiyuki Suda,[a] Atsushi Ozeki, Hirotake Sugawara, and Yosuke Sakai
Division of Electronics for Informatics, Graduate School of Information Science and Technology, Hokkaido University, N14 W9, Sapporo 060-0814, Japan

Akinori Oda
Graduate School of Engineering, Nagoya Institute of Technology Gokiso-cho, Showa-ku, Nagoya 466-8555, Japan

Junji Nakamura
Graduate School of Pure and Applied Sciences, University of Tsukuba, Tennoudai 1-1-1, Tsukuba, Ibaraki 305-8573, Japan

(Received 14 June 2005; accepted 16 November 2005; published online 3 January 2006)

Carbon nanotubes (CNTs) were grown on Si substrates by rf CH_4 plasma-enhanced chemical vapor deposition in a pressure range of 1–10 Torr, and then characterized by scanning electron microscopy. At 1 Torr, the CNTs continued growing up to 60 min, while their height at 4 Torr had leveled off at 20 min. CNTs hardly grew at 10 Torr and amorphous carbon was deposited instead. CH_4 plasma was simulated using a one-dimensional fluid model to evaluate the production and transport of radicals, ions, and nonradical neutrals. The amount of simulated carbon supplied to the electrode surface via the flux of radicals and ions such as CH_3, C_2H_5, and $C_2H_5^+$ was consistent with estimations from experimental results. © *2006 American Institute of Physics*.
[DOI: 10.1063/1.2150599]

I. INTRODUCTION

Carbon nanotubes (CNTs) have excellent physical and electronic properties such as high electrical conductivities, field emission capabilities, and tensile strengths, and are widely studied for various possible applications, e.g., field electron emitters, scanning probes, and electronic devices.[1] Among various CNT production methods, plasma-enhanced chemical vapor deposition (PECVD) is an advantageous technique because it can yield vertically aligned single/multiwalled CNTs (SWNTs/MWNTs) and carbon nanofibers (CNFs) at low substrate temperatures [T_{sub}=550 °C for SWNTs,[2] ~280 °C,[3] 370 °C (Ref. 4) for MWNTs, and 120 °C for CNFs (Ref. 5)]. Low temperature operation is crucial for the application of CNTs in LSIs. While it is often mentioned that the electron-impact dissociation of hydrocarbons and the generation of radicals in plasmas lowers the CNT growth temperature, it is still unclear how the plasma contributes to the CNT growth through the radical production.

To investigate the role of plasma in PECVD of CNTs, diagnostics utilizing optical emission spectroscopy (OES) and mass spectrometry have been extensively carried out, as has plasma modeling.[6–11] OES has an advantage in its spatial resolution of the measurements, while mass spectrometry can detect even nonradiative species of high molecular weight. Plasma modeling is suitable for analysis of the overall behavior of plasma species. Denysenko *et al.*[10] analyzed an inductively coupled $Ar/CH_4/H_2$ plasma for PECVD of vertically aligned carbon nanostructures using quadrupole mass spectrometry and OES, and compared the results of the number densities of neutrals and ions with estimations by a zero-dimensional rate equation. Delzeit *et al.*[6] used a zero-dimensional model to characterize CH_4/H_2 plasmas for CNT growth and suggested enhancement in CH_4 dissociation by collision of H atoms. Hash *et al.*[8] performed one-dimensional simulations of dc $C_2H_2/NH_3/Ar$ plasmas for CNT production. They revealed the effect of dc bias by examining electron temperatures and densities of electrons, ions, and neutrals. Examples of modeling of CH_4 plasmas, like the present work, are also found in literature on the deposition of carbon films[12–14] although their CH_4 pressure ranges (p_{CH_4}=10–250 mTorr) are relatively lower than that suitable for CNT growth (1–10 Torr).

To understand the mechanism of CNT growth and controlling CNT characteristics, we focused our discussion on carbon-containing species. Eres *et al.*[15] showed the tendency for the relative fraction of small-diameter CNTs to increase with the incidence rate of carbon-containing molecules. Their results indicate the possibility of controlling CNT characteristics by external tuning of the carbon supply. Estimation of the carbon amount in CNTs and plasma gas-phase enables us to obtain insights into the mechanisms of CNT growth with respect to the following points: (1) interaction of plasma gas-phase with catalyst material and catalyst activity; (2) identification of precursor species for CNT growth; (3) evaluation of the sticking probability of radicals on a catalyst surface; and (4) the effect of various process parameters.

In this study, we analyzed the amount of carbon deposited on the substrate from the experimental results of PECVD performed at p_{CH_4}=1–10 Torr. Using scanning electron microscopy (SEM), we measured the length, diam-

[a]Electronic mail: suda@ist.hokudai.ac.jp

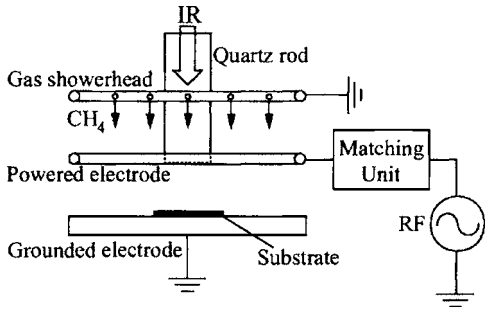

FIG. 1. The electrode configuration of the PECVD system.

eter and number density of the deposited CNTs. We compared these experimental results with computational estimations from the fluxes of precursor species onto the substrate, using one-dimensional plasma fluid modeling. The effect of p_{CH_4} on CNT growth is discussed from the viewpoint of the quantitative estimation of the carbon supply.

II. EXPERIMENTAL DETAILS

Figure 1 shows a schematic of the configuration of the present electrodes set in a SUS reactor with an inner diameter of 20.3 cm and a height of 27.6 cm. The separation d between the powered and the grounded electrodes is 1.5 cm, and the distance between the ring gas showerhead and the powered electrode is also 1.5 cm. This showerhead uniformly feeds CH_4 for deposition and H_2 for reduction of catalysts. The powered electrode is a circular plate 8.0-cm in diameter with a hole 2.5 cm in inner diameter, through which a quartz rod 2.3 cm in diameter guides the infrared (IR) to heat the substrate. The diameter of the grounded electrode is 6.4 cm. The lower end of the quartz rod is 1.5 cm apart from the grounded electrode, on which Si substrates are placed. The substrate temperature T_{sub} is kept constant by a temperature controller (Thermo Riko Co. Ltd., GVL298) with a thermocouple. The powered electrode is connected to a 13.56 MHz rf generator (RF Power Products Inc., RFPP-RF5S) through a matching unit (ASTECH Corp., RC-11 and TH-5R). The plasma ignites between the electrodes and the gases are fed with their flow rates controlled by mass flow controllers (STEC Inc., SEC-400). The gas pressure is measured with a capacitance manometer (Megatorr Corp., COLD-31S07E).

By an electron beam evaporator (ULVAC Inc., EBV-6DA), a three-layered catalyst film (Al_2O_3/Fe/Al_2O_3, 3 nm/3 nm/3 nm) was deposited onto Si substrates (N-doped, ⟨100⟩) with a 15 nm thick SiO_2 layer. During the preparation, the film thickness is monitored by a quartz crystal deposition controller (ULVAC Inc., CRTM-5000). Fe works as a catalyst for CNT growth, and Al_2O_3 is a catalyst support.[16] The three-layered structure is suitable to obtain nanometer-sized catalyst particles.[17]

In the experiment, the reactor was first pumped down to about 10^{-6} Torr. Next, the Si substrate on the grounded electrode was heated to 500 °C in 1 min in H_2 gas (H_2 99.99999% pure) at 4–5 Torr. Then, the catalyst was reduced in H_2 plasma for 10 min. After that, T_{sub} was increased to 650 °C, CH_4 (99.99% pure) was introduced, and p_{CH_4} was set at the desired values. The growth time T was 3–60 min in the present experiment. After deposition, any CH_4 remaining in the reactor was purged by H_2 to avoid deposition of amorphous carbon during the cooling process that followed. Then, plasma and the IR light were turned off. H_2 was fed until T_{sub} reached 300 °C. Note that we had confirmed that CNTs do not grow in CH_4 (without plasma) even at T_{sub} = 650 °C. Other experimental conditions are listed in Table I. The CNTs obtained were characterized using a SEM (Hitachi High-Technologies Corp., S-4800).

TABLE I. Experimental conditions.

Process	Parameter	Value
Reduction	H_2 pressure	4–5 Torr
	H_2 flow rate	50 sccm
	Input power	50 W
	Period	10 min
Growth	CH_4 pressure	1–10 Torr
	CH_4 flow rate	30 sccm
	Input power	100 W
	Period	3–60 min

III. PLASMA MODELING

We analyzed the carbon sources in CH_4 plasmas (p_{CH_4} = 1–10 Torr, gas temperature = 650 °C) using a one-dimensional fluid model in the x direction; the electrode configuration is shown in Fig. 2. The simulation consists of calculations of continuity equations, Poisson's equation, and an electron energy conservation equation. The detail of the numerical scheme is based on earlier works.[18–21] The number densities n_j of electrons, neutrals and ions (subscript j represents species) are calculated spatiotemporally by the following continuity equations:

$$\frac{\partial n_j}{\partial t} + \nabla \Gamma_j = S_j, \tag{1}$$

$$\Gamma_j = z_j n_j \mu_j E - D_j \nabla n_j, \tag{2}$$

where Γ_j is the flux. S_j is the source term representing the production and consumption of particles through reactions. E is the electric field, z_j is the sign to distinguish the species (electrons and negative ions: $z_j = -1$, positive ions: $z_j = +1$, neutrals: $z_j = 0$), μ_j is the mobility, and D_j is the diffusion coefficient.

E is given as $E = -\nabla V$ from the following Poisson's equation:

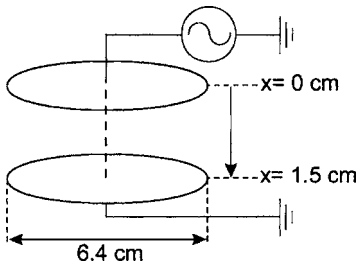

FIG. 2. The electrode configuration assumed in the simulation.

$$\nabla^2 V = -\frac{e}{\epsilon_0}(n_+ - n_-), \tag{3}$$

where V is the potential in the gap between the electrodes, e is the elementary charge, ϵ_0 is the permittivity of free space, and n_+ and n_- are the total numbers of the densities of positively and negatively charged particles, respectively.

The mean electron energy $\bar{\epsilon}$ ($=\frac{3}{2}k_B T_e$ where k_B is the Boltzmann constant and T_e is the electron temperature) is determined by the following electron energy conservation equation:

$$\frac{\partial}{\partial t}\left(n_e \frac{3}{2} k_B T_e\right) + \nabla q_e = -e\Gamma_e E + S_{\text{energy}}, \tag{4}$$

where q_e is the total energy flux determined by the following equation:

$$q_e = \frac{5}{3}\Gamma_e \frac{3}{2} k_B T_e - \frac{5}{3} n_e D_e \left(\nabla \frac{3}{2} k_B T_e\right). \tag{5}$$

The boundary conditions at the electrode surfaces ($x=0, d$) for Eqs. (1) and (2) were, respectively, taken as

$$\Gamma_e(x=0,d) = -\gamma_{\text{ion}}\Gamma_+, \tag{6}$$

$$\Gamma_+(x=0,d) = -\mu_+ n_+ \nabla V, \tag{7}$$

$$V(0) = V_{\text{rf}} \sin(2\pi f t), \tag{8}$$

$$V(d) = 0. \tag{9}$$

Here, γ_{ion} is the secondary electron emission coefficient, V_{rf} is the amplitude of the applied rf voltage (400–670 V, with a constant power density=0.36 W/cm^3), and f is the power source frequency (13.56 MHz). At the electrode surface, reflection and loss of radicals, CH, CH_2, CH_3, C_2H_5, and H are assumed, and their sticking coefficients are 0.025, 0.025, 0.01, 0.01, and 0.01, respectively.[10]

The input parameter of this model, the electron drift velocity W_e, and the rate coefficients k of electron-CH_4 reactions were obtained from a Boltzmann equation analysis using a set of the electron collision cross sections of CH_4.[22] The reaction rate coefficients k for H_2, CH_2, CH_3, C_2H_2, C_2H_4, C_2H_5, C_2H_6 were estimated from their reaction cross sections.[10,23,24] The mobilities and diffusion coefficients of charged species, except electron mobility, the secondary electron emission coefficient ($\gamma_{\text{ion}}=0.01$), the initial energy for secondary electrons (=1.0 eV), the detachment coefficient ($=3.69\times10^{-11}$ cm^3/s) and the recombination coefficient (=0.0 cm^3/s) are cited from Gogolides *et al.*[20] D_j of neutral species in the CH_4 plasma were calculated as referred to in Herrebout *et al.*[25] An overview of the species (nonradical neutrals, ions, radical neutrals) taken into account in the present model is given in Table II. The reaction processes among electrons, ions, excited atoms and molecules taken here and their reaction rate coefficients are listed in Tables III–V: 28 for electron-neutral, 15 for ion-neutral, and 25 for neutral-neutral reactions.

TABLE II. Ionic and neutral species taken into account in the simulation.

Particle	Species
Nonradical neutral	H_2, CH_4, C_2H_2, C_2H_4, C_2H_6, C_3H_8
Ion	H_2^+, CH_2^+, CH_3^+, CH_4^+, CH_5^+, $C_2H_2^+$, $C_2H_4^+$, $C_2H_5^+$, $C_2H_6^+$, CH_2^-, H^-
Radical neutral	H, CH, CH_2, CH_3, C_2H_5

IV. RESULTS AND DISCUSSIONS

A. SEM analysis of CNT growth

Figure 3 shows SEM micrographs of the CNTs growth at $p_{CH_4}=1-10$ Torr for 10 min. The CNTs grown at 1 Torr are vertically well aligned with a high density. At 4 Torr, CNTs are longer than those grown at 1 Torr; however, their number density is less than at 1 Torr and the CNTs appear entangled. CNTs hardly grew at 10 Torr under the present experimental conditions.

Lin *et al.*[27] performed CNT growth by electron cyclotron resonance and microwave PECVDs with CH_4/H_2 at 2.3–4.5 mTorr and 4.5–25 Torr, respectively, and noted a great amount of carbon supply and random orientation at high pressures. Delzeit *et al.*[6] grew CNFs using a CH_4/H_2 inductively coupled plasma across a pressure range of 0.5–20 Torr, and reported that the number density of CNFs obtained below 1 Torr was low and that amorphous carbon was deposited at high pressures. These tendencies for pres-

TABLE III. Electron reactions with molecules.

Reaction	Reference
$CH_4+e^- \rightarrow CH_4^*+e^-$ (2 vib.)[a]	21
$CH_4+e^- \rightarrow CH_4^+ + 2e^-$	21
$CH_4+e^- \rightarrow CH_3^+ + H + 2e^-$	21
$CH_4+e^- \rightarrow CH_3 + H + e^-$	21
$CH_4+e^- \rightarrow CH_2 + 2H + e^-$	21
$CH_4+e^- \rightarrow CH + 3H + e^-$	21
$CH_4+e^- \rightarrow CH + 3H + e^-$	21
$CH_4+e^- \rightarrow CH_3 + H^-$	21
$CH_4+e^- \rightarrow CH_2^- + 2H$	21
$H_2+e^- \rightarrow H_2^+ + 2e^-$	10 and 23
$H_2+e^- \rightarrow 2H + e^-$	10 and 23
$CH_2+e^- \rightarrow CH_2^+ + 2e^-$	10 and 24
$CH_2+e^- \rightarrow CH + H + e^-$	10 and 24
$CH_3+e^- \rightarrow CH_3^+ + 2e^-$	10 and 24
$CH_3+e^- \rightarrow CH_2 + H + e^-$	10 and 24
$CH_3+e^- \rightarrow CH + 2H + e^-$	10 and 24
$C_2H_2+e^- \rightarrow C_2H_2^*+e^-$ (3 vib.)[a]	10 and 24
$C_2H_2+e^- \rightarrow C_2H_2^+ + 2e^-$	10 and 24
$C_2H_4+e^- \rightarrow C_2H_4^*+e^-$ (2 vib.)[a]	10 and 24
$C_2H_4+e^- \rightarrow C_2H_4^+ + 2e^-$	10 and 24
$C_2H_4+e^- \rightarrow C_2H_2 + 2H + e^-$	10 and 24
$C_2H_5+e^- \rightarrow C_2H_5^+ + 2e^-$	10 and 24
$C_2H_5+e^- \rightarrow C_2H_4^+ + H + 2e^-$	10 and 24
$C_2H_5+e^- \rightarrow C_2H_4 + H + e^-$	10 and 24
$C_2H_6+e^- \rightarrow C_2H_6^+ + 2e^-$	10 and 24
$C_2H_6+e^- \rightarrow C_2H_5^+ + H + 2e^-$	10 and 24
$C_2H_6+e^- \rightarrow C_2H_5 + H + e^-$	10 and 24
$C_2H_6+e^- \rightarrow C_2H_4 + 2H + e^-$	10 and 24

[a]vib.: vibrational excited state.

TABLE IV. Ion-neutral reactions (Ref. 10).

Reaction	Rate coefficient ($cm^3\ s^{-1}$)
$CH_3^+ + CH_4 \rightarrow CH_4^+ + CH_3$	1.36×10^{-10}
$CH_3^+ + CH_4 \rightarrow C_2H_5^+ + H_2$	1.2×10^{-9}
$CH_4^+ + CH_4 \rightarrow CH_5^+ + CH_3$	1.5×10^{-9}
$CH_4^+ + H_2 \rightarrow CH_5^+ + H$	3.3×10^{-11}
$CH_5^+ + C_2H_6 \rightarrow C_2H_5^+ + CH_4 + H_2$	5.0×10^{-10}
$C_2H_2^+ + CH_4 \rightarrow C_2H_3^+ + CH_3$	4.1×10^{-9}
$C_2H_2^+ + CH_4 \rightarrow C_3H_4^+ + H_2$	6.25×10^{-10}
$C_2H_2^+ + CH_4 \rightarrow C_3H_5^+ + H$	1.44×10^{-9}
$C_2H_4^+ + C_2H_4 \rightarrow C_3H_5^+ + CH_3$	3.9×10^{-10}
$C_2H_4^+ + C_2H_4 \rightarrow C_4H_8^+$	4.3×10^{-10}
$C_2H_4^+ + C_2H_6 \rightarrow C_3H_6^+ + CH_4$	2.03×10^{-13}
$C_2H_4^+ + C_2H_6 \rightarrow C_3H_7^+ + CH_3$	1.32×10^{-11}
$C_2H_5^+ + C_2H_2 \rightarrow C_4H_7^+$	6.7×10^{-10}
$C_2H_5^+ + C_2H_4 \rightarrow C_3H_5^+ + CH_4$	3.1×10^{-10}
$C_2H_5^+ + C_2H_4 \rightarrow C_4H_9^+$	3.0×10^{-10}

sure dependence, i.e., the CNT orientation and production of amorphous carbon, were also observed in the present experiments with CH_4.

The length, diameter, and number density of CNTs at different CNT growth times T evaluated from the SEM images are shown in Fig. 4. At $p_{CH_4}=1$ Torr, CNTs grew linearly up to $T=60$ min. CNTs grown at 4 Torr are longer than those at 1 Torr; however, the growth leveled off at about $T=20$ min, when the length was about 6 μm. After $T=20$ min at 4 Torr, CNTs grew in diameter but not in length. In the SEM analysis done in the present work, a lot of amorphous carbon was observed as deposited on the upper ends and sidewalls of CNTs for $T>10$ min at 4 Torr. It is thought that CNT growth stopped at a certain T and that deposition of amorphous carbon started instead, because the tips of the CNTs were thickly covered by amorphous carbon at $T=60$ min. A similar feature, that CNTs keep growing at low pressures and stop growing at high pressures, is seen for C_2H_2/NH_3; Chhowalla *et al.*[28] reported that CNTs continued growing for 30 min (4 Torr, dc plasma). On the other hand, the experiment by Bower *et al.*[29] showed that CNTs stopped growing around 5 min (20 Torr, microwave PECVD). These results indicate the presence of a pressure factor that limits CNT growth.

The CNT number density at 1 Torr had its peak of $\sim1.4\times10^{11}$ cm^{-2} at $T=10$ min and decreased thereafter. Its value was about twice that at 4 Torr. The CNT number density at 4 Torr seems almost constant at around 3.4×10^{10} cm^{-2} irrespective of T. Gas pressure seems to be a critical parameter in CNT growth by PECVD.

The present experimental data of the length, diameter and number density of CNTs is used later to calculate the amount of C deposited.

B. Simulation results

Figure 5(a) shows the fluxes of primary species flowing onto the surface of the grounded electrode (average over an rf cycle) at $p_{CH_4}=1-10$ Torr. The fluxes of C_2H_4, C_2H_6, C_3H_8, and H_2 increased with p_{CH_4}. On the other hand, those of positive ions, C_2H_5, CH_3, CH_2, CH, H, and C decreased.

TABLE V. Neutral-neutral reactions. T_{gas} is the gas temperature in K.

Reaction	Rate coefficient ($cm^3\ s^{-1}$)	Reference
$CH_3 + H \rightarrow CH_4$	7.0×10^{-12}	25
$CH_3 + H \rightarrow CH_2 + H_2$	$1.0\times10^{-10}\exp(-7600/T_{gas})$	10
$CH_3 + C \rightarrow C_2H_2 + H$	8.3×10^{-11}	26
$CH_3 + CH \rightarrow C_2H_3 + H$	5.0×10^{-11}	10
$CH_3 + CH_2 \rightarrow C_2H_4 + H$	3.3×10^{-11}	25
$CH_3 + CH_3 \rightarrow C_2H_6$	3.7×10^{-11}	25
$CH_3 + CH_3 \rightarrow C_2H_5 + H$	$5.0\times10^{-11}\exp(-6800/T_{gas})$	10
$CH_3 + CH_3 \rightarrow C_2H_4 + H_2$	$1.7\times10^{-8}\exp(-16000/T_{gas})$	10
$CH_3 + C_2H_5 \rightarrow C_3H_8$	4.2×10^{-12}	25
$CH_2 + H \rightarrow CH + H_2$	2.7×10^{-10}	25
$CH_2 + CH \rightarrow C_2H_2 + H$	6.6×10^{-11}	10
$CH_2 + CH_2 \rightarrow C_2H_2 + H_2$	1.1×10^{-11}	25
$CH_2 + CH_2 \rightarrow C_2H_4$	1.7×10^{-12}	10
$CH_2 + CH_4 \rightarrow 2CH_3$	1.7×10^{-11}	25
$CH_2 + CH_4 \rightarrow C_2H_4 + H_2$	1.7×10^{-11}	25
$CH_2 + C_2H_6 \rightarrow C_3H_8$	4.0×10^{-10}	10
$CH + CH \rightarrow C_2H_2$	2.0×10^{-10}	10
$CH + CH_4 \rightarrow C_2H_5$	1.0×10^{-10}	25
$CH + CH_4 \rightarrow C_2H_4 + H$	1.0×10^{-10}	10
$H + CH_4 \rightarrow CH_3 + H_2$	$2.2\times10^{-20}(T_{gas})^3\exp(-4045/T_{gas})$	10
$H + C_2H_2 \rightarrow C_2H + H_2$	$1.0\times10^{-10}\exp(-14000/T_{gas})$	10
$H + C_2H_4 \rightarrow C_2H_3 + H_2$	$9.0\times10^{-10}\exp(-7500/T_{gas})$	10
$H + C_2H_5 \rightarrow C_2H_4 + H_2$	5.0×10^{-11}	10
$H + C_2H_5 \rightarrow 2CH_3$	6.0×10^{-11}	10
$H + C_2H_6 \rightarrow C_2H_5 + H_2$	$2.4\times10^{-15}(T_{gas})^{1.5}\exp(-3730/T_{gas})$	10

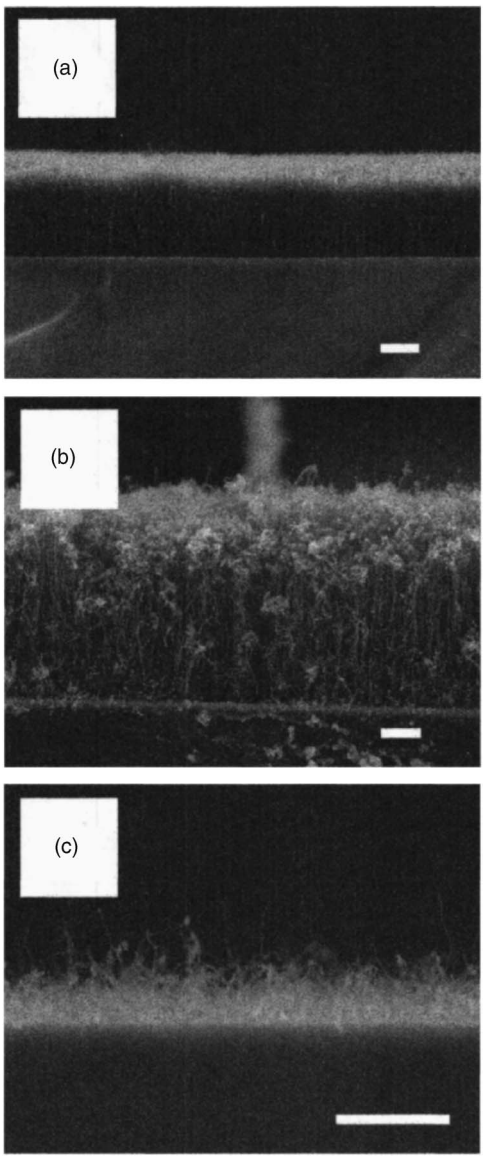

FIG. 3. SEM micrographs of CNTs grown for 10 min at p_{CH_4} of (a) 1 Torr, (b) 4 Torr, and (c) 10 Torr. Scale bar, 1 μm.

Among these species, CH_2, CH, and H decreased for recombination processes listed in Table V to produce species with high molecular weights.

In the present analysis, C_2H_4, CH_3, C, and C_2H_5 were the major neutrals as shown in Fig. 5(b). C_2H_4 was produced through the recombination of CH_3, CH_2, and CH. Among the radicals, the absolute densities of CH_3 and C_2H_5 were 2–3 orders of magnitude higher than those of CH_2 and CH. The quantitative order of the fluxes, $\Gamma_{C_2H_4} > \Gamma_{CH_3} > \Gamma_{C_2H_2} > \Gamma_{C_2H_6} > \Gamma_{CH_2} > \Gamma_{CH}$, is similar to the results by Tachibana *et al.*[30] Considering the factors of the sticking coefficients of radicals,[10] it is speculated that the positive ions, CH_3 and C_2H_5 are main species that fulfill the role of supplying carbon to the substrate in the present modeling.

C. Estimation of carbon amount

We estimated the number of C atoms per unit substrate area and compared the values of the experimental and simulation results, N_C and N'_C, respectively. For the calculation of N_C, we assumed that each MWNT has 6 layers, from an additional observation by transmission electron microscopy, and that its interlayer distance is 0.335 nm. A graphene sheet contains C atoms of 3.81×10^{15} cm^{-2} theoretically. Data of the mean CNT length, the outer diameter and the number

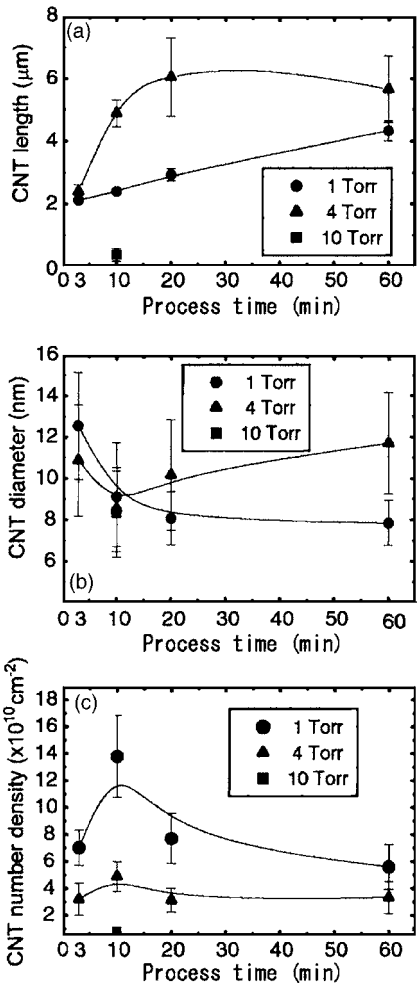

FIG. 4. Experimental results of (a) the length, (b) the diameter, and (c) the number density of CNTs grown at $p_{CH_4} = 1-10$ Torr.

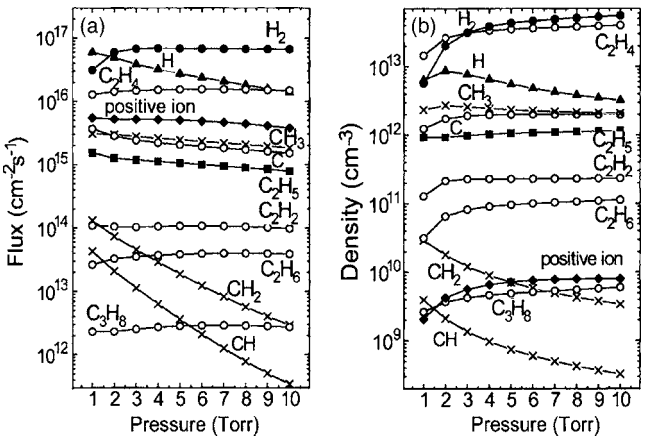

FIG. 5. Pressure dependence of the time-averaged fluxes and the number densities of species in the CH_4 plasmas at $p_{CH_4} = 1-10$ Torr; (a) fluxes flowing onto the substrate surface and (b) number densities averaged over the electrode gap.

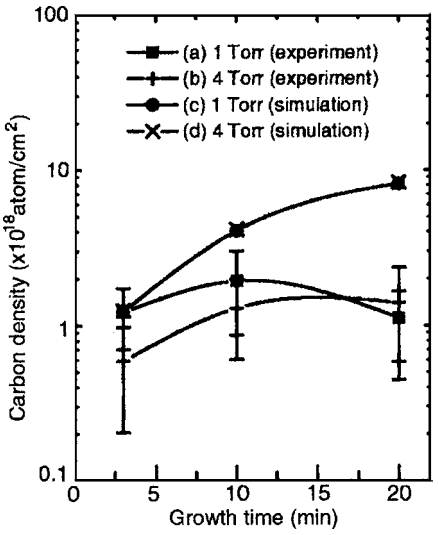

FIG. 6. Number density of carbon atoms: experimental results for the CNTs grown at 1 Torr and 4 Torr (full squares and plus signs), and simulation results for those supplied as radicals and nonradical neutrals at 1 Torr and 4 Torr (full circles and crosses).

density were taken from Fig. 4. N'_C was given as the C amount per unit area supplied as radicals and ions from the CH_4 plasma. We integrated the fluxes of radicals, ions, and nonradical neutrals incident on the surface of the substrate during the growth time T. Their sticking coefficients s_j are assumed to be $s_{CH}=0.025$, $s_{CH_2}=0.025$, $s_{CH_3}=0.01$, $s_{C_2H_5}=0.01$, and s_n (nonradicals neutrals)$=0$.[10] The sticking coefficients of ions is set at $s_{ion}=1$.[31] N'_C is given as $N'_C=\Sigma_j C_j s_j \Gamma_j T$, where C_j is the carbon atom content in species j (e.g., $C_{C_xH_y}=x$).

N_C and N'_C calculated for $p_{CH_4}=1$ and 4 Torr and $T=3-20$ min are shown in Fig. 6. The present estimation shows that N_C is of the same order of magnitude as N'_C. The shortage of N_C relative to N'_C would be due to the loss caused by the production of amorphous carbon, and, crucially, the surface coverage ratio of catalyst would affect the experiments.

V. CONCLUSIONS

We performed CNT growth experiments by CH_4 PECVD at $p_{CH_4}=1-10$ Torr, and investigated the contributions of radicals and ions to CNT growth by simulating CH_4 plasma using a one-dimensional fluid model.

At 1 Torr, CNTs continued growing up to 60 min. At 4 Torr, CNTs grew longer and thicker than at 1 Torr; however, their length had leveled off by 20 min and their density was lower than at 1 Torr. CNTs hardly grew at 10 Torr. These results indicate that an optimum value exists for the carbon supply for CNT growth, and that an oversupply of carbon induces the production of amorphous carbon.

The simulation showed the pressure dependence of the fluxes of plasma species to the substrate surface. The carbon supply estimated from the simulation results, even by a simple model, was consistent with the amount of deposited carbon as calculated from the experimental results.

In the present simulation, the sticking coefficients of the nonradical neutrals were treated to be zero in spite of their high fluxes into the substrate. For further realistic evaluations of CNT growth from the viewpoint of carbon supply, more detailed information on the surface reactions of nonradical neutrals as well as that for radicals and ions will be necessary.

ACKNOWLEDGMENTS

Work by A. Okita was supported under a 21st century COE program, "Meme-Media Technology Approach to the R&D of Next-Generation Information Technologies" and a Grant-in-Aid (16760240) by MEXT and The Ushio Foundation, Japan. The authors acknowledge provision of the experimental facility by Professors T. Fukui and K. Sueoka at Hokkaido University and Dr. J. Tsujino at Hokkaido Electric and Power Corporation, and valuable discussions on PECVD experiments and plasma modeling with Professor Z. F. Ren at Boston College and Dr. D. Hash at NASA.

[1] J. Han, in *Carbon Nanotubes: Science and Applications*, edited by M. Meyyappan (CRC, Boca Raton, 2005), Chap. 1.
[2] T. Kato, G. H. Jeong, T. Hirata, R. Hatakeyama, K. Tohji, and K. Motomiya, Chem. Phys. Lett. **381**, 422 (2003).
[3] M. Chen, C. M. Chen, S. C. Shi, and C. F. Chen, Jpn. J. Appl. Phys., Part 1 **42**, 614 (2003).
[4] J. M. Ting and K. H. Liao, Chem. Phys. Lett. **396**, 469 (2004).
[5] S. Hofmann, C. Ducati, J. Robertson, and B. Kleinsorge, Appl. Phys. Lett. **83**, 135 (2003).
[6] L. Delzeit, I. McAnich, B. A. Cruden, D. Hash, B. Chen, J. Han, and M. Meyyappan, J. Appl. Phys. **91**, 6027 (2002).
[7] D. B. Hash and M. Meyyappan, J. Appl. Phys. **93**, 750 (2003).
[8] D. Hash, D. Bose, T. R. Govindan, and M. Meyyappan, J. Appl. Phys. **93**, 6284 (2003).
[9] M. Meyyappan, L. Delzeit, A. Cassell, and D. Hash, Plasma Sources Sci. Technol. **12**, 205 (2003).
[10] I. B. Denysenko, S. Xu, J. D. Long, P. P. Rutkevych, N. A. Azarenkov, and K. Ostrikov, J. Appl. Phys. **95**, 2713 (2004).
[11] B. A. Cruden, A. M. Cassell, D. B. Hash, and M. Meyyappan, J. Appl. Phys. **96**, 5284 (2004).
[12] N. V. Mantzaris, E. Gogolides, A. G. Boudouvis, A. Rhallabi, and G. Turban, J. Appl. Phys. **79**, 3718 (1996).
[13] D. J. Dagel, C. M. Mallouris, and J. R. Doyle, J. Appl. Phys. **79**, 8735 (1996).
[14] K. Nagayama, B. Farouk, and Y. H. Lee, IEEE Trans. Plasma Sci. **26**, 125 (1998).
[15] G. Eres, A. A. Kinkhabwala, H. Cui, D. B. Geohegan, A. A. Puretzky, and D. H. Lowndes, J. Phys. Chem. B **109**, 16684 (2005).
[16] R. Y. Zhang, I. Amlani, J. Baker, J. Tresek, and R. K. Tsui, Nano Lett. **3**, 731 (2003).
[17] G. Zhong, T. Iwasaki, K. Honda, Y. Furukawa, I. Ohdomari, and H. Kawarada, Chem. Vap. Deposition **11**, 127 (2005).
[18] A. Oda, Y. Sakai, H. Akashi, and H. Sugawara, J. Phys. D **32**, 2726 (1999).
[19] D. P. Lymberopoulos and D. J. Economou, J. Appl. Phys. **73**, 3668 (1993).
[20] E. Gogolides, C. Buteau, A. Rhallabi, and G. Turban, J. Phys. D **27**, 818 (1994).
[21] E. Gogolides, D. Mary, A. Rhallabi, and G. Turban, Jpn. J. Appl. Phys., Part 1 **34**, 261 (1995).
[22] D. K. Davies, L. E. Kline, and W. E. Bies, J. Appl. Phys. **65**, 3311 (1989).
[23] http://www.kinema.com/download.htm
[24] D. A. Alman, D. N. Ruzic, and J. N. Brooks, Phys. Plasmas **7**, 1421 (2000).
[25] D. Herrebout, A. Bogaerts, M. Yan, R. Gijbels, W. Goedheer, and E. Dekempeneer, J. Appl. Phys. **90**, 570 (2001).
[26] N. A. Morrison, C. William, and W. I. Milne, J. Appl. Phys. **94**, 7031 (2003).
[27] C. H. Lin, S. H. Lee, C. M. Hsu, and C. T. Kuo, Diamond Relat. Mater. **13**, 2147 (2004).

[28]M. Chhowalla, K. B. K. Teo, C. Ducati, N. L. Rupesinghe, G. A. J. Amaratunga, A. C. Ferrari, D. Roy, J. Robertson, and W. I. Milne, J. Appl. Phys. **90**, 5308 (2001).
[29]C. Bower, O. Zhou, W. Zhu, D. J. Werder, and S. Jin, Appl. Phys. Lett. **77**, 2767 (2000).
[30]K. Tachibana, M. Nishida, H. Harima, and Y. Urano, J. Phys. D **17**, 1727 (1984).
[31]W. Jacob, Thin Solid Films **326**, 1 (1998).